Electroreduction of $SOCl_2$
I. $AlCl_3$-$SOCl_2$ System on Pt Electrode

P. A. Mosier-Boss* and S. Szpak*

Naval Ocean Systems Center, San Diego, California 95152-5000

J. J. Smith

Department of Energy, Washington, DC 20545

R. J. Nowak*

Office of Naval Research, Arlington, Virginia 22217-5000

ABSTRACT

The mechanism of $SOCl_2$ reduction on Pt electrodes is examined by linear sweep voltammetry and IR reflectance spectroscopy with the interpretation aided by molecular orbital calculations. The present model emphasizes structural aspects of bulk electrolyte as well as the electrode/electrolyte interphase region. Initially this region is enriched by preferential adsorption of $[Cl_2Al(\leftarrow OSCl_2)_2]^+$ ions occurring through the S atom of the complexed $SOCl_2$ molecule. Further enhancement is noted at low cathodic overpotentials. At higher overpotentials, SO_2 and unidentified species, P_1 and P_2, are observed. The model requires stability of both P_1 and P_2 when in an adsorbed state. The acceptance of the first electron is an irreversible process while the acceptance of the second electron is quasi-reversible. The formation of final reaction products, *viz.*, Cl^-, S, and SO_2 occurs within the reaction layer.

Early discussion of the mechanism of $SOCl_2$ electroreduction centered around events involving isolated $SOCl_2$ molecules, *i.e.*, disregarding molecular interactions (1-4). This approach was criticized by Madou *et al.* (5) based on the shape of voltammograms, particularly in practical electrolytes containing excess $AlCl_3$. The complexity of the reaction path was indicated by the formation of prepassive surface films long before the onset of passivation (6) and further emphasized by the role played by the various additives, *e.g.*, Fe-Pc (7). However, the best evidence for the complex reaction pathway was provided by the spectroscopic examination of the Pt/$AlCl_3$-LiCl-$SOCl_2$ interphase region (8, 9).

In an attempt to provide better understanding of events associated with the cell discharge and, in particular, those occurring at the positive electrode, studies into the structural aspects of $SOCl_2$-based electrolytes were undertaken (10-12). Specifically, structural features were derived from the analysis of the Walden product (10) and from Raman and IR spectra for the $AlCl_3$-$SOCl_2$ and LiCl-$AlCl_3$-$SOCl_2$ systems, respectively (11, 12). Here, we report on the extension of this effort and concentrate on changes that occur within the reaction zone adjacent to the charge-transfer plane upon polarization of the Pt/$AlCl_3$-$SOCl_2$ system. IR reflectance spectroscopy and linear sweep voltammetry (lsv) were selected as primary experimental tools. The interpretation of experimental observations was aided by molecular orbital (MO) calculations.

Experimental

Procedures employed in the preparation of solutions were reported earlier (11, 12). The spectroscopic examination of the electrode/electrolyte interphase was performed in a modified cell, first described by Pons (13). The linear sweep voltammograms were obtained with the aid of the computer driven potentiostat, PAR Model 173 with a 276 IEEE computer interface. IR transmittance spectra were obtained using a Barnes mount with AgCl windows and a 15 μm Teflon space. The MO calculations were performed using AMPAC, a general purpose, semiempirical molecular orbital package developed at the University of Texas, Austin, Texas. These calculations yield information on the size, shape, and charge distribution within molecules and complexes. The recorded S—O stretching vibrations of complexed $SOCl_2$ were computer analyzed and decomposed into their Voigt profiles using a previously described procedure (14).

Electrochemical cell.—The spectroelectrochemical cell was made of a machinable ceramic material (Macor, Dow Chemical). A removable AgCl window was sealed against the cell body by an O-ring (Kalrez, du Pont). The working electrode was a polished Pt foil permanently attached to a ceramic plunger. The counter- and reference electrodes were a Pt wire and a Ag/AgCl wire in a Teflon sleeve, respectively. A variable distance between the window and electrode surface was provided; however, each set of measurements was carried out at a fixed distance. The cell was placed at a 45° angle using a specular reflectance apparatus—Spectra-Tech, Model 500—inside a 5 DXB Nicolet FT-IR spectrometer. The path lengths were calibrated with neat CCl_4.

Results

IR spectra can be used to identify species present in solution and, to a lesser degree, determine their concentrations. Such an examination by itself can, at best, provide only limited information on the characteristics of the electrode/electrolyte interphase (15); it cannot unequivocally determine the reaction pathway(s). On the other hand, linear sweep voltammetry is a useful tool for exploring complex electrochemical processes since the shape of the lsv curves depends on two parameters related to the thermodynamics of the system and to the kinetics of the charge transfer and associated transport processes. Moreover, the easily adjustable experimental conditions allow the examination of a transition from one dominant process to another.

IR spectroscopy of the electrode/electrolyte interphase.—The evolution of IR spectra reflected from the electrode surface is illustrated in Fig. 1. Detailed examination was restricted to the spectral region: 950-1350 cm^{-1}. This region was selected because the S—O stretching vibrations of neat $SOCl_2$, $Cl_3Al(\leftarrow OSCl_2)$ complex and $[Cl_2Al(\leftarrow OSCl_2)_2]^+$ onium ion, which occur in the Raman spectra at 1231, 1108, and 1055 cm^{-1}, respectively, are unobstructed by other absorptions. Also, the S—O stretching vibrations of these species are very sensitive to any changes in the molecular structure (11). For solutions in contact with an electrode surface two additional peaks at 1132 and 1102 cm^{-1} are observed (*vide infra*). The passage of cathodic current results in the disappearance of the 1132 and 1102 cm^{-1} peaks and generates new peaks of which that of SO_2 at 1331 cm^{-1}, is clearly detectable, even at low overpotentials, *e.g.*, 100 mV. At higher overpotentials, new peaks appear at *ca.* 1190, 1170, and 1150 cm^{-1}. Qualitatively, no significant differences are observed in the IR reflectance spectra obtained on Au and Pt electrodes.

lsv curves.—Effect of $AlCl_3$ concentration.—The effect of $AlCl_3$ concentration on the shape of the lsv curves, re-

* Electrochemical Society Active Member.

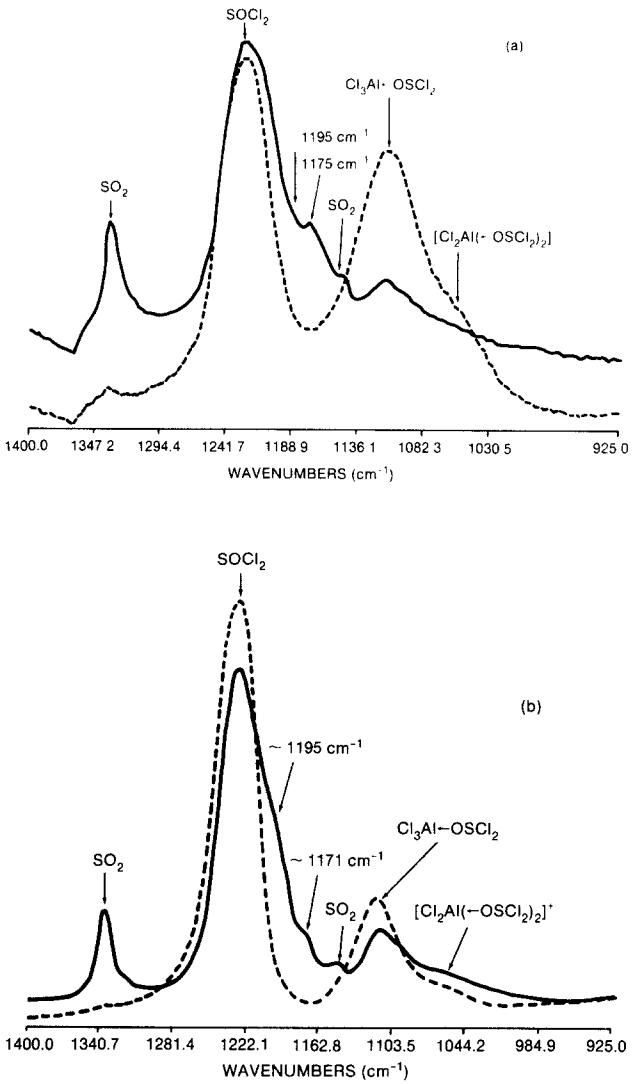

Fig. 1. The 930-1350 cm^{-1} IR spectral region of an electrode/electrolyte interphase at rest and cathodically polarized. (a) Au/4.0M $AlCl_3$ in $SOCl_2$ system; dashed line at $\eta = 0$, solid line at $\eta = -2.5$V. (b) Pt/4.0M $AlCl_3$ in $SOCl_2$ system; dashed line at $\eta = 0$, solid line at $\eta = -3.5$V. Species indicated.

corded for a constant scan rate of 5 mV s^{-1}, is illustrated in Fig. 2a-d. A cursory inspection shows a significant difference. On closer examination, however, this difference is in the definition of characteristic points rather than in shape. At concentrations 3.0*M* or less, the forward (reductive) scan consists of two S-shaped segments, followed by a peak current. The current plateaus, j_A and j_B, as well as the peak current, j_p, increase with an increase in $AlCl_3$ concentration. The reverse (oxidative) scan also exhibits two S-shaped segments followed by a rather distinctly different region containing two peaks. All potentials delineating the characteristic segments appear to be concentration independent while the respective currents show a strong dependence.

The situation in a 4.0*M* solution, especially at higher overpotentials, is quite different both on forward and reverse scans. The reductive scan shows only one wave-shaped region at lower overpotentials, becoming a straight line at higher overpotentials. On reverse scan, the $j/V(t)$ curve crosses over the reductive scan, but still retains a peak-shaped region at lower overpotentials.

lsv curves.—Effect of scan rate.—The effect of scan rate on the shape of the lsv curves in a 3.0*M* solution is illustrated in Fig. 3a and b. Qualitatively, the decrease in the scan rate yields better definition of the various regions. Thus, at $\nu < 50$ mV s^{-1}, all characteristic features of both reductive and oxidative scans are clearly displayed. Of interest are two features: the merging of the reductive and oxidative waves within the potential range: −500 to −200 mV at the scan rate of 5 mV s^{-1}. At still lower rates a cross over of oxidative and reductive waves is observed while at faster rates, a separation of these waves occurs. The second feature of interest is the behavior of peaks, A and B in Fig. 3a. As the scan rate decreases, merging of these points occurs with A shifting in the positive direction and B in the negative, with the displacement of the latter being less.

Discussion

The discussion of experimental results and conclusions reached is aided by considerations of electrolyte composition and associated equilibria and the concept of an electrode/electrolyte interphase.

*Equilibria in the bulk electrolyte.*Mosier-Boss *et al.* (11) reported the following equilibria in the bulk solution

$$(SOCl_2)_n \leftrightarrows (SOCl_2)_{n-1} \quad n = 1, 2, \ldots \qquad [I]$$

$$SOCl_2 + AlCl_3 \leftrightarrows Cl_3Al(\leftarrow OSCl_2) \qquad [II]$$

$$2Cl_3Al(\leftarrow OSCl_2) \leftrightarrows [Cl_2Al(\leftarrow OSCl_2)_2]^+ + AlCl_4^- \qquad [III]$$

The internal exchange reaction, Eq. [III], occurs in the presence of free $SOCl_2$ and the extent of this reaction is expected to be affected by excess $SOCl_2$ with a dependence on the dielectric constant at low $AlCl_3$ concentrations and dominated by the donor properties of the $SOCl_2$ at higher concentrations (16). Significant changes in the governing equilibria and molecular structure occur between 2.0 and 3.0*M* $AlCl_3$ as indicated by difference in IR spectra (8) and a maximum in the electrolyte vapor pressure (17). (Hereafter, for brevity, we use symbols A_0, A_1, and A_2^+ to denote neat $SOCl_2$, complex, and onium ion, respectively).

Concept of an interphase.—A useful concept facilitating the interpretation of experimental data and formulation of a physical model, that of an interphase region, was discussed by van Rysselberghe (18). In the simplest case, it takes the form of the electrical double layer. In more complex cases and, in particular, during charge transfer reaction, it consists of a series of layers, each associated with a participating elementary process. In this representation, the interphase region is an open system which encompasses a number of consecutive elementary processes. A typical set of events is as follows; reactant molecules are brought from the bulk, b, to the electrode surface, s, by diffusion, d, followed by adsorption, a, and, after the charge transfer, products are returned back to the bulk. For A_2^+ as the reacting molecule, the set of events is given by Eq. [IV]

$$A_2^{+,(b)} \rightarrow A_2^{+,(d)} \rightarrow A_2^{+,(a)} + e^{-,(s)} \rightarrow \Sigma \text{ products} \qquad [IV]$$

where the superscripts identify the elementary process considered as well as their position within the interphase.

An interphase region is formed whenever an electrode is in contact with an electrolyte. This region is either in an equilibrium with the bulk electrolyte or in a stationary state leading to a rest potential which is a thermodynamic or a mixed potential, respectively. In the first case, the constituents within the interphase are the same as in the bulk, while in the second case new species are generated by the partial electrode reactions. These new species, depending upon their stability, may or may not have time to diffuse to the bulk.

IR spectroscopy of the interphase region.—In the cell designed for external reflection spectroelectrochemistry, the recorded spectra contain contributions due to bulk electrolyte and the electrode/electrolyte interphase (13). The degree to which the interphase region can be isolated from the bulk, and events associated with the charge transfer process examined, can be assessed by, *e.g.*, varying the path length. The effectiveness of this technique is illustrated by spectra displayed in Fig. 4. Figures 4a and b are the spectra for path lengths of 5 and 10 μm, respectively; relative intensities between the two cases reflect bulk *vs.* interphase concentrations. The peak ratios of complexed species, *i.e.*, onium ion, A_2^+, and complex, A_1, to free $SOCl_2$, increase with decreasing cell path length which is

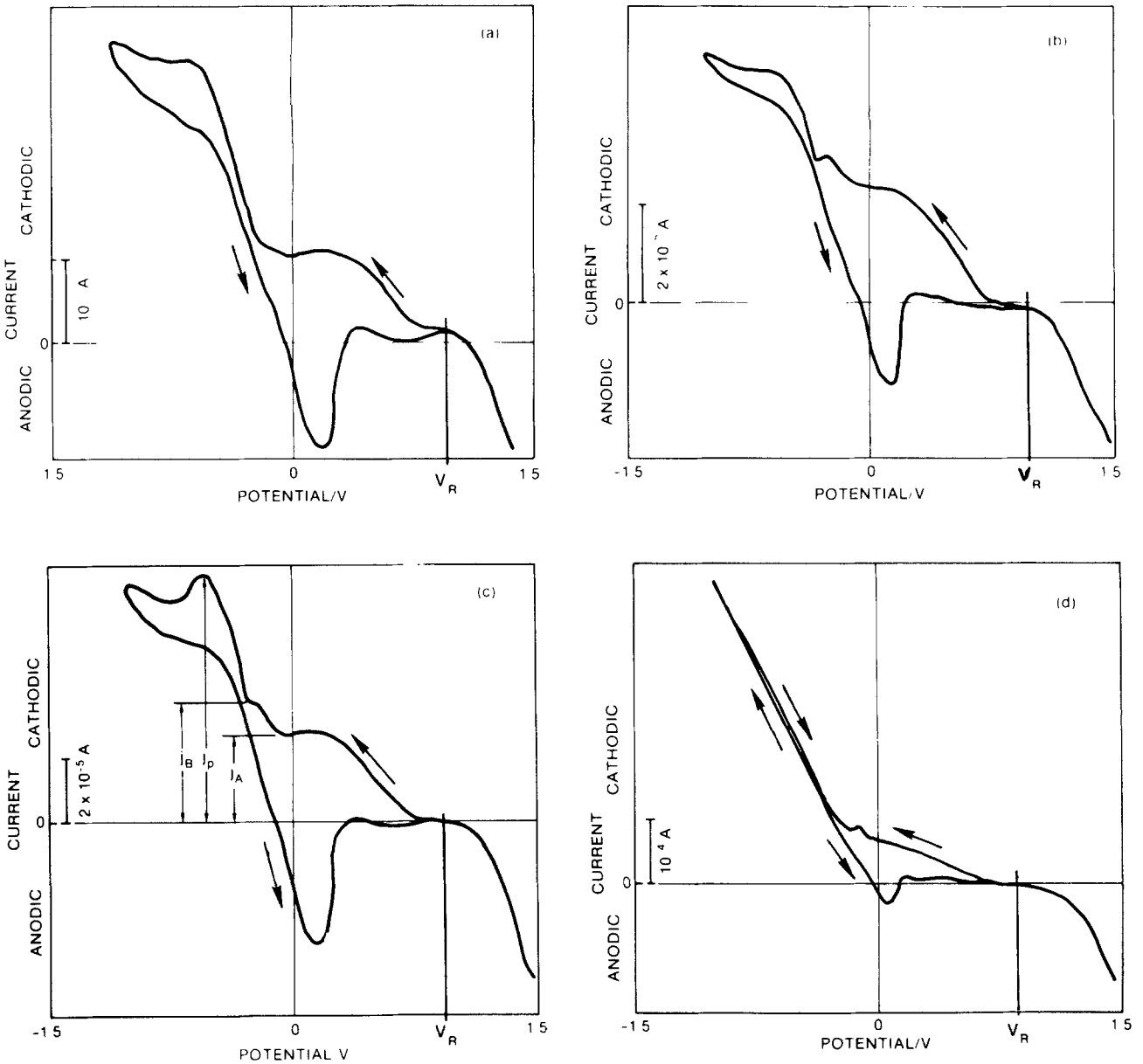

Fig. 2. Effect of $AlCl_3$ concentration on shape of voltammograms. (a) 1.5M; (b) 2.0M; (c) 3.0M; (d) 4.0M $AlCl_3$. Scan rate: $\nu_{red} = \nu_{ox} - 5$ mV s^{-1}. Electrode area: 0.15 cm^2. All potentials vs. Ag/AgCl reference in the same solution. V_R indicates rest potential.

indicative of enrichment of the former within the interphase. A more quantitative demonstration of the interphase enrichment can be seen in Fig. 5 and Table I where the resolved Voigt profiles for the S—O vibration band at 1116 cm^{-1} are displayed. It should be noted that both the transmittance and reflectance IR spectra were obtained using AgCl windows. Consequently, the observed effects are due to the electrode/electrolyte interphase and not an artifact of the AgCl windows.

The Voigt profiles show two new peaks at 1132 and 1102 cm^{-1} which are present only within the interphase. These peaks disappear upon cathodic polarization. Two plausible assignments can be made: (*i*) they can be assigned to the symmetric and asymmetric stretching vibrations of $A_2^{+,(a)}$ or (*ii*) to S—O stretching vibrations of $A_1^{(a)}$ and $A_2^{+,(a)}$, respectively. In the first case, these vibrations in the bulk solution are essentially degenerate and appear as a broad band. Case (*ii*) is consistent with the observation that A_2^+ is more strongly enriched within the interphase than A_1. Further distinction between these two cases cannot be made at the present time. Regardless, since these peaks are shifted to higher frequencies, it follows that the adsorption occurs through the S atom. A shift to higher frequency requires an increase in the force constant of the S—O bond which can only occur if the $p\pi \rightarrow d\pi$ backbonding increases. This conclusion is based on the thoroughly investigated effects of bonding through the S and O atoms of $(CH_3)_2SO$ on the S—O stretching frequencies (19, 20), and further supported by MO calculations. These calculations show that the positive charge rests on the S atom (12). For case (*i*), the removal of degeneracy would imply that only one of the $SOCl_2$ molecules of the onium ion is actually on the electrode surface.

In summary, the *in situ* IR reflectance spectroscopy clearly indicates that we have a complex electrode/electrolyte interphase. This interphase consists of onium ions (and possibly, 1:1 adduct) adsorbed on the electrode surface in contact with a region of enrichment of onium ions and complex which, in turn, is in contact with the bulk.

Shape of lsv curves.—The tendency of $SOCl_2$ to form adducts and/or to solvate ions further suggests that the electroreduction of $SOCl_2$ in practical electrolytes comprises a complex overall reaction where, most likely, chemical reaction(s) is (are) coupled to a charge transfer. For this reason, the lsv is the experimental technique of choice to assess the complexity of this reaction and elucidate, at least in a qualitative manner, its mechanism. This approach is based on the premise that, for a specific coupling, a characteristic lsv curve is obtained (21, 22). The shape of this curve depends on two parameters: the thermodynamic parameter, $\chi = Kc$, and the kinetic parameter,

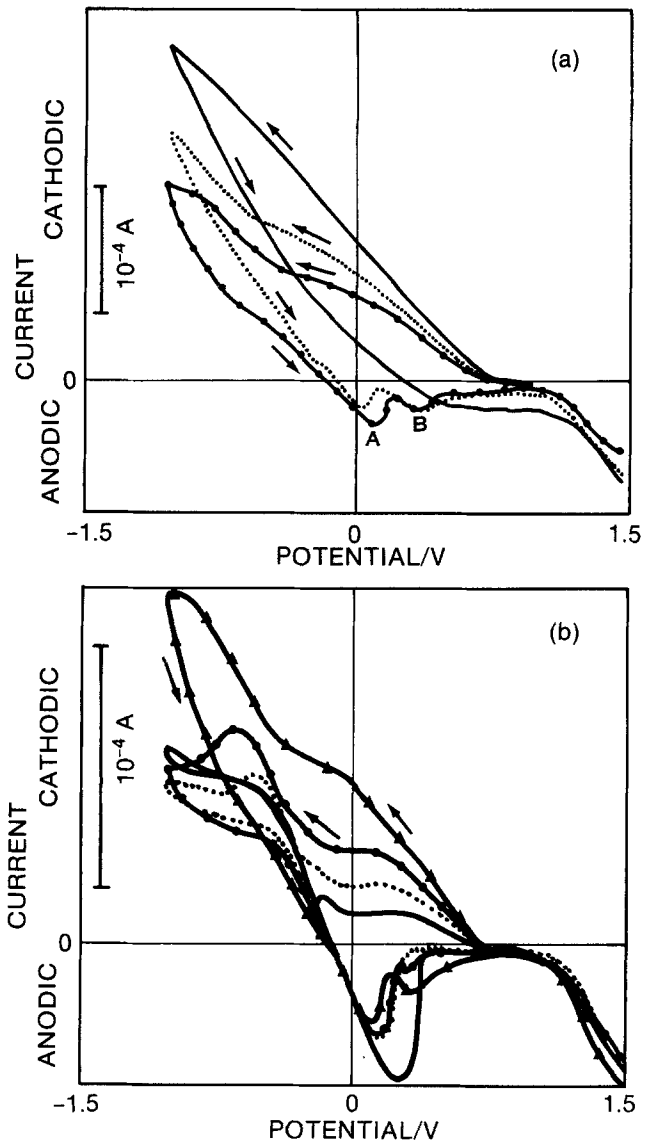

Fig. 3. Effect of scan rate on shape of voltammograms. (a) Scan rates: $\nu_{red} = \nu_{ox} > 50$ mV s^{-1} (———) for 500; (····) for 100, and (–·–·–·–) for 50 mV s^{-1}. (b) Scan rates; $\nu_{red} = \nu_{ox} < 50$ mV s^{-1} (———) for 2; (····) for 5; (–·–·–·–) for 10, and (———) for 50 mV s^{-1}. Electrolyte, 3.0*M* $AlCl_3$. Electrode area: 0.15 cm^2.

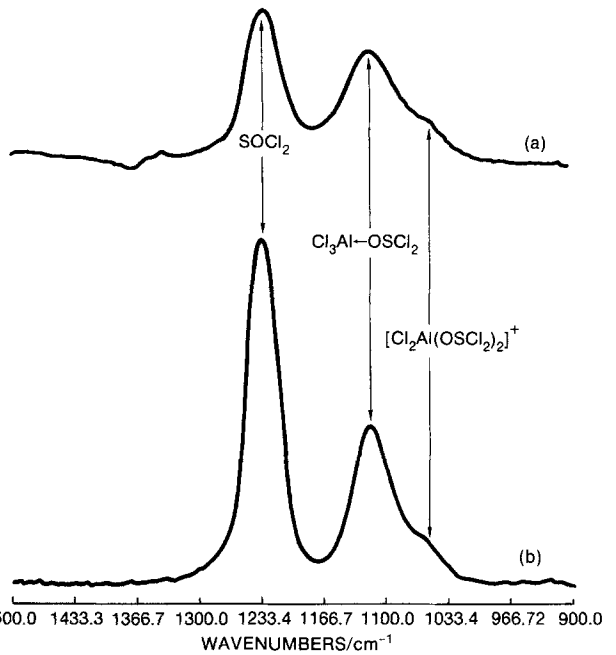

Fig. 4. IR reflectance spectra at rest potential. (a) and (b) Reflectance spectrum as a function of path lengths of 5 and 10 μm, respectively. Electrolyte, 4.0*M* $AlCl_3$ in $SOCl_2$; electrode material, Au.

$\lambda = (RT/n\mathbf{F})\, c(k/\nu)$. These parameters enter as a source/sink term in the mass balance equation, Eq. [1]

$$\frac{\partial c_i}{\partial t} = D_i \frac{\partial^2 c_i}{\partial x^2} - f_i(\chi, \lambda) \qquad [1]$$

where c_i is the concentration of the i-th electroactive species, K is the equilibrium constant, k is the appropriate rate constant, and ν the scan rate. The source/sink function, $f_i(\chi, \lambda)$, is formulated for a specific set of events comprising the overall reaction. Any discussion of the reaction mechanism(s), even a qualitative one, must involve specification of the $f_i(\chi, \lambda)$ function which, in turn, requires an examination of the effect of solution composition and the scan rate. Often, this function is potential dependent and may be simplified by making relevant approximations. Because of the low conductivity of these electrolytes, any attempt for a quantitative evaluation of kinetic factors would not be appropriate (23-25) and, therefore, has not been pursued further. It is emphasized that the shape of the lsv is determined solely by the mass balance equation, Eq. [1]. The resistivity of the electrolyte enters through the λ parameter and affects the position and the symmetry of the peak current as well as its magnitude. In particular, anodic peaks are displaced in the positive direction while the cathodic peaks in the more negative direction (24).

In principle, solution of Eq. [1], subject to appropriate initial and boundary conditions, implies that all pertinent information can be derived from the analysis of a single scan. For complex reactions, however, additional information can be extracted by scan reversal, especially if adsorbed species participate in the charge transfer. This assertion is demonstrated in Fig. 6 where the shape of the j/V curve produced by the reverse scan depends on the point of termination of the forward scan. For example, when the forward scan is reversed at point A, the j/V curves on the forward and reverse scan coincide. At higher cathodic overpotentials, points B, C, and D, the oxidative segments of the j/V curves differ substantially from those on the forward scan. These differences can be used in the formulation of a reaction pathway.

Initial stages of lsv curves.—The rather significant enhancement in the concentration of A_2^+ in the vicinity of the electrode surface both at rest potential and while cathodically polarized, is illustrated in Fig. 7, where the reference spectrum obtained at rest potential has been subtracted

Table I. Decomposition of spectral bands of free and adsorbed complexed $SOCl_2$ into Voigt profiles

Method[a]	Symbol[b]	Complex (Bulk)	Onium ion		
			Bulk	Adsorbed state	
T	ν_0	1116.92	1065.55	—	—
	$\Delta\nu_G$	6.085	36.535	—	—
	$\Delta\nu_L$	44.296	61.382	—	—
	I_0	1.137	0.142	—	—
	A	80.175	16.277	—	—
R/Pt	ν_0	1116.96	1064.79	1132.25	1102.97
	$\Delta\nu_G$	9.335	60.260	24.036	26.640
	$\Delta\nu_L$	32.896	6.350	6.302	11.364
	I_0	0.046	0.022	0.018	0.029
	A	2.505	1.589	0.578	1.185
R/Au	ν_0	1116.26	1060.11	1132.92	1101.40
	$\Delta\nu_G$	8.536	57.589	28.128	29.628
	$\Delta\nu_L$	53.452	3.868	8.866	16.616
	I_0	0.080	0.033	0.016	0.037
	A	6.823	2.135	0.647	1.847

[a] T—transmittance
R—reflectance
[b] $\Delta\nu_G$—Gassian width, cm^{-1}
$\Delta\nu_L$—Lorentzian width, cm^{-1}
I_0—peak intensity, Abs
A—band area, Abs cm^{-1}
ν_0—peak position, cm^{-1}

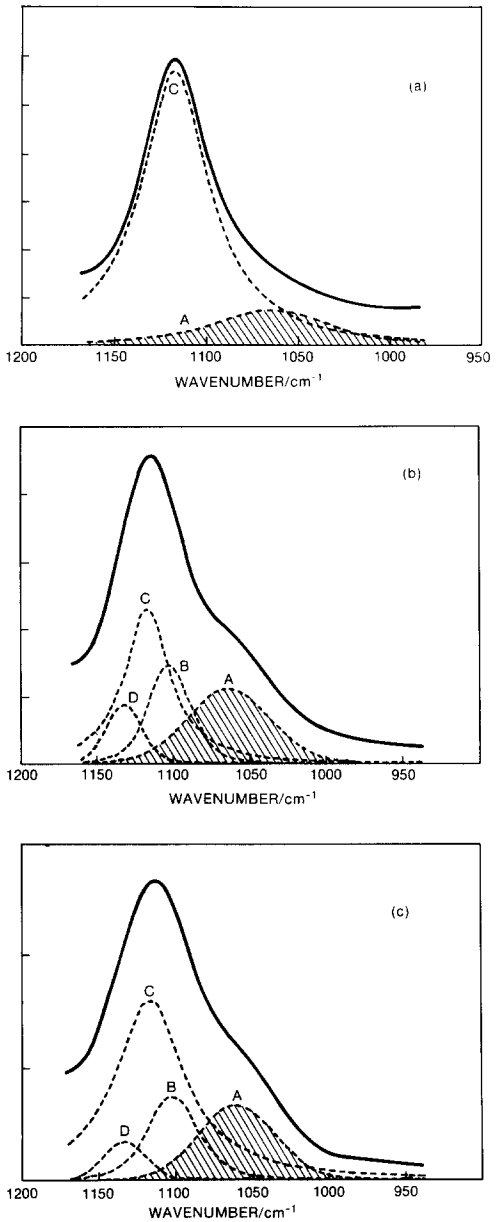

Fig. 5. The 950-1150 cm^{-1} IR special region decomposed into Voigt profiles. (a) Transmittance spectrum, (b) reflectance spectrum from Au electrode, (c) reflectance spectrum from Pt electrode. Both at V_R. A, C, S—O vibrations due to onium and complex in the bulk; B, D, asymmetric and symmetric S—O stretching vibrations of the adsorbed onium ions, respectively, or S—O stretching vibrations of adsorbed onium ion and 1:1 complex, respectively. Electrolyte, 4.0M $AlCl_3$ in $SOCl_2$.

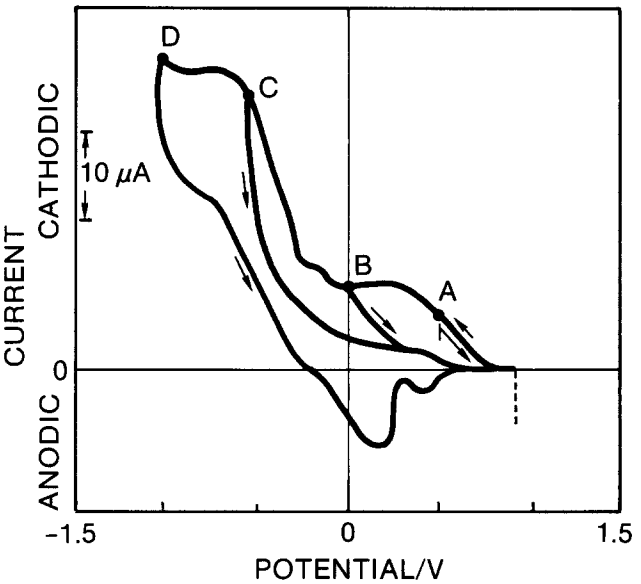

Fig. 6. Effect of scan reversal potential on the shape of $J/V(t)$ curves. Electrolyte, 1.5M $AlCl_3$ in $SOCl_2$; scan rate $\nu_{ox} = \nu_{red} = 5$ mV s^{-1}; points; A, B, C, and D indicate scan reversal.

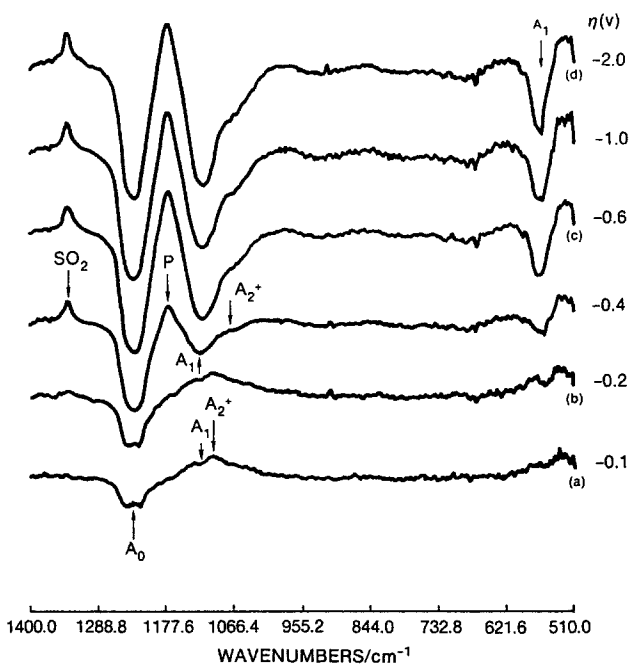

Fig. 7. Effect of applied overpotential on the composition of the interphase by subtractive IR spectroscopy. Electrolyte, 4.0M $AlCl_3$ in $SOCl_2$.

out. (Figure 1 shows the S—O stretching spectral region for the polarized and unpolarized cases, *vide supra.*) There is a corresponding displacement of A_0 and A_1. Evidently, at low overpotentials, *i.e.*, when the charge transfer reaction is insignificant, the major event is the potential dependent shift in the equilibria, Eq. [I]-[III], taking place within the confines of the interphase region. With a further passage of current, new peaks appear, *viz.*, at 1331 and *ca.* 1150 cm^{-1} due to the formation of SO_2 and at 1170 and 1190 cm^{-1} assigned to, as yet, unidentified products containing a S—O bond with the peak at 1170 cm^{-1} appearing first. It is noteworthy that these peaks are not due to SO_2 complexes with either $SOCl_2$ or $AlCl_3$. Concurrently, there is the loss of A_0, A_1, and A_2^+ species, indicated in Fig. 7 by the negative peaks at 1231, 1108, and 1055 cm^{-1}, respectively. It is not clear, however, whether the $SOCl_2$ in these species are simultaneously reduced or if only one species, *e.g.*, A_2^+, participates in the reduction process. This ambiguity cannot be resolved by kinetic arguments alone because the species present are coupled to one another via the chemical equilibria, Eq. [II] and [III], and products of the electroreduction of one species may shift the equilibrium to regenerate the electroreducible species. However, assuming the discharge from either species can occur independently, the MO calculations favor the discharge from the A_2^+ species, Eq. [V]

$$A_2^+ + e^- \rightarrow P_1 \quad k_1, V^0_1, \alpha_1 \qquad [V]$$

This conclusion is consistent with data asssembled in Tables II-IV. As indicated, the calculated heats of formation for the addition of an electron to A_1 and A_2^+ are −132 and −299 kcal/mol, respectively. Assuming P_1 to be the initial reaction product, it is likely that the 1190 and/or 1170 cm^{-1} bands in the IR, Fig. 1, are associated with it or with P_2 (*vide infra*, Eq. [VI]). Furthermore, on the basis of the coincidence of the forward and reversed lsv , Fig. 6, point A, we conclude that the charge transfer reaction, Eq. [V], is irreversible.

Development of current plateau(s).—The characteristic feature of the reductive lsv is the appearance of a current

Table II. Bond length and charge density distribution following electron acceptance by neat $SOCl_2$

Reactions

$SOCl_2$; $\Delta H_f = -22$ kcal/mol
$SOCl_2 + e^- \rightarrow SOCl_2^-$; $\Delta H_f = -111$ kcal/mol
$SOCl_2^- + e^- \rightarrow SOCl_2^{2-}$; $\Delta H_f = -48$ kcal/mol
(ΔH_f is the MO calculated heat of formation from the elements)

Bond lengths, Å

Bond	$SOCl_2$	$SOCl_2^-$	$SOCl_2^{2-}$
S—O	1.468	1.477	1.492
S—Cl_1	2.037	2.160	2.452
S—Cl_2	2.038	2.161	2.453

Charge density

Atom	$SOCl_2$	$SOCl_2^-$	$SOCl_2^{2-}$
S	1.2349	0.9203	0.4708
O	−0.5500	−0.5644	−0.7369
Cl_1	−0.3424	−0.6789	−0.8669
Cl_2	−0.3425	−0.6790	−0.8670

Table III. Bond length and charge density distribution following electron acceptance by 1:1 complex

Reactions

$Cl_3Al \leftarrow OSCl_2$; $\Delta H_f = -178$ kcal/mol
$Cl_3Al \leftarrow OSCl_2 + e^- \rightarrow Cl_3Al \leftarrow OSCl_2^-$; $\Delta H_f = -309$ kcal/mol
$Cl_3Al \leftarrow OSCl_2^- + e^- \rightarrow Cl_3Al \leftarrow OSCl_2^{2-}$; $\Delta H_f = -309$ kcal/mol
(ΔH_f is the MO calculated heat of formation from the elements)

Bond lengths, Å

Bond	$Cl_3Al \leftarrow OSCl_2$	$Cl_3Al(\leftarrow OSCl_2)^-$	$Cl_3Al(\leftarrow OSCl)_2)^{2-}$
S—O	1.496	1.5315	1.560
S—Cl_1	2.020	2.056	2.179
S—Cl_2	2.018	2.055	2.179
O—Al	1.845	1.7436	1.673
Al—Cl_3	2.103	2.154	2.182
Al—Cl_4	2.107	2.143	2.183
Al—Cl_5	2.127	2.137	2.187

Charge density

Atom	$Cl_3Al(\leftarrow OSCl_2)$	$Cl_3Al(\leftarrow OSCl_2)^-$	$Cl_3Al(\leftarrow OSCl)_2)^{2-}$
S	1.3293	0.9872	0.6609
O	−0.6238	−0.6592	−0.6791
Al	0.9616	0.9859	1.0317
Cl_1	−0.2235	−0.4461	−0.6966
Cl_2	−0.2217	−0.4472	−0.6973
Cl_3	−0.4382	−0.4884	−0.5378
Cl_4	−0.3975	−0.4718	−0.5378
Cl_5	−0.3861	−0.4604	−0.5440

plateau extending over a considerable range of overpotentials, *cf.* Fig. 2. The development of such a current plateau in lsv experiments suggests coupling of chemical reaction(s) to the charge transfer. More specifically, the coupling reaction must either precede or be in parallel with the charge transfer. For the ce-type reaction, the current plateau is proportional to the concentration of the electroactive species, here A_2^+, but independent of the scan rate. The experimental evidence presented in Fig. 3, is in agreement with the first but not the second condition, if the charge transfer reaction is irreversible. The situation is less clear if the charge transfer reaction is reversible or if it occurs in parallel (21). In the simplest case, the appearance of the current plateau for an exponential $j = f(V)$ relationship, requires that the depletion of the electroactive species is balanced by its production within the zone adjacent to the electrode surface. Otherwise, with an increase in overpotential (and, in the lsv experiments, also with time) the condition $\partial A_2^+/\partial t = 0$ cannot be realized.

With the further increase in cathodic overpotentials, yet another current plateau appears, Fig. 2b. This current plateau occurs within a much narrower potential range and is better defined at slower scan rates and lower $AlCl_3$ concentrations. While the coupling of reaction, Eq. [III] with the charge transfer, Eq. [IV], is presumed to be responsible for the development of the first current plateau, the conditions for the development of the second plateau cannot be, at the present time, as clearly stated. However, if the interphase region is considered an open system, the condition of constant affinity exists and can be specified by thermodynamic reasoning, provided that the necessary information is available (18, 26). Analogous to the development of the first plateau, the appearance of the second plateau may be attributed to the coupling of adsorption and charge transfer to the chemical reaction and diffusion. Occurrence of chemical reaction(s) requires the presence of reaction layer, r, sandwiched between the adsorption and diffusion layers.

Table IV. Bond length and charge density distribution following electron acceptance by onium ion

Reactions

$Cl_2Al(\leftarrow OSCl_2)_2^+$; $\Delta H_f = -11$ kcal/mol
$Cl_2Al(\leftarrow OSCl_2)_2^+ + e^- \rightarrow Cl_2Al(\leftarrow OSCl_2)_2$; $\Delta H_f = -310$ kcal/mol
$Cl_2Al(\leftarrow OSCl_2)_2 + e^- \rightarrow Cl_2Al(\leftarrow OSCl_2)_2^-$; $\Delta H_f = -347$ kcal/mol
(ΔH_f is the MO calculated heat of formation from the elements)

Bond lengths, Å

Bond	$Cl_2Al \leftarrow OSCl_2)_2^+$	$Cl_2Al(\leftarrow OSCl_2)_2$	$Cl_2Al(\leftarrow OSCl)_2)_2^-$
S_1—O_1	1.506	1.496	1.534
S_1—Cl_1	2.010	2.013	2.053
S_1—Cl_2	2.103	2.018	2.049
Al—O_1	1.795	1.844	1.737
Al—Cl_3	2.093	2.108	2.145
Al—Cl_4	2.096	2.121	2.147
Al—O_2	1.785	1.688	1.737
O_2—S_2	1.510	1.534	1.533
S_2—Cl_5	2.009	2.031	2.053
S_2—Cl_6	2.012	2.052	2.050

Charge density

Atom	$Cl_2Al(\leftarrow OSCl_2)_2^+$	$Cl_2Al(\leftarrow OSCl_2)_2$	$Cl_2Al(\leftarrow OSCl)_2)_2^-$
Al	1.1016	1.116	1.081
O_1	−0.6868	−0.635	−0.6719
O_2	−0.6836	−0.737	−0.6728
S_1	1.3343	1.336	1.007
S_2	1.3265	1.044	1.007
Cl_1	−0.1579	−0.225	−0.450
Cl_2	−0.1711	−0.218	−0.444
Cl_3	−0.3666	−0.407	−0.480
Cl_4	−0.3691	−0.432	−0.482
Cl_5	−0.1585	−0.3913	−0.450
Cl_6	−0.1686	−0.4501	−0.444

Reversal of the reductive scan at potentials within the current plateau, *e.g.*, at point B, Fig. 6, results in a decrease in the charge transfer current density which can be attributed to blocking of the electrode surface by an adsorbed species, $P_2^{(a)}$, generated by a slow reduction of P_1, Eq. [VI]

$$P_1^{(a)} + e^- \rightarrow P_2^{(a)} \qquad k_{-2} >> k_2;\ V_2^0,\ \alpha_2 \qquad [VI]$$

The participation of an adsorption step becomes quite evident at higher overpotentials. Qualitatively, the presence of an adsorption step is illustrated in Fig. 6 where a plot of the oxidative lsv is displayed as a function of terminating potential of the reductive scan. The oxidative lsv exhibits two broad peaks whose currents increase with the terminating voltage, without substantial changes in their potentials, however. Such a behavior leads to the following conclusions: (*i*) as the overpotential increases so does the accumulation of reaction product(s) at the electrode surface, and (*ii*) these product(s) are reoxidized within the potential range 200-1000 mV. Thus, the charge transfer reaction, Eq. [VI], is quasi-reversible.

Elementary processes at higher overpotentials.—The current/time relationship, $j(0, t)$, for $V(t) = V_i + |\nu|t$, for the N electroactive species and M adsorption processes, is given by Eq. [2]

$$j(0, t) = \mathbf{F}\left[\sum_{i=1}^{N} n_i D_i \frac{\partial c_i}{\partial x} + \sum_{m=1}^{M} \Gamma_m \frac{d\theta_m}{dt}\right] \qquad [2]$$

where Γ_m denotes the maximum surface concentration of the m-th species. Both terms in Eq. [2] are time dependent, but in a different way. At slow scan rates, transport of reac-

tants and products between the bulk and the interphase is substantial and the observed lsv is sensitive to the scan rate. At fast scan rates, the condition at the electrode surface is the dominant factor and the contribution due to transport is minimal. As a general observation, the scan rate of $\nu = 100$ mV s^{-1} is taken as the rate separating these contributions (27).

The composition of the interphase region, arising from the interplay between the electrode surface processes and the bulk, is determined by the reductive scan rate and the terminal potential. To illustrate, we selected two scan rates, *viz.*, 5 and 100 mV s^{-1}, with the terminal voltage at −1200 mV. In accordance with Eq. [2], the slower scan includes the effect of transport on surface processes while the faster scan focuses on the processes pertinent to the adsorbed species. Even a cursory examination of Fig. 8a and b, reveals that a slow reductive scan promotes the accumulation of reaction product that can be reoxidized.

The surface condition generated by the slow and fast reductive scan are examined via the analysis of the oxidative lsv. In particular, Fig. 9a-d show the response of the electrode/electrolyte interphase generated at a slow reductive scan and Fig. 10a-d, for fast scans. It is seen that the interphase generated at slow scan rate is insensitive to the oxidative scan rates throughout the potential range. Differences only appear within the potential range of anodic currents. The response of the interphase generated at fast scan rate is more complex, *viz.*, high scan rates affect the region of anodic currents while slow rates influence processes immediately after scan reversal. Such a behavior is

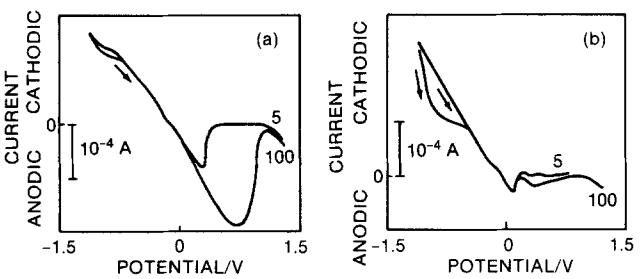

Fig. 8. Effect of reductive scan rate on the composition of the interphase displayed by oxidative lsv at $\nu_{ox} = 5$ and 100 mV s^{-1} (a) for $\nu_{red} = 10$ mV s^{-1}; (b) for $\nu_{red} = 100$ mV s^{-1}. Electrolyte, 3.0M $AlCl_3$ in $SOCl_2$; ν_{ox} indicated.

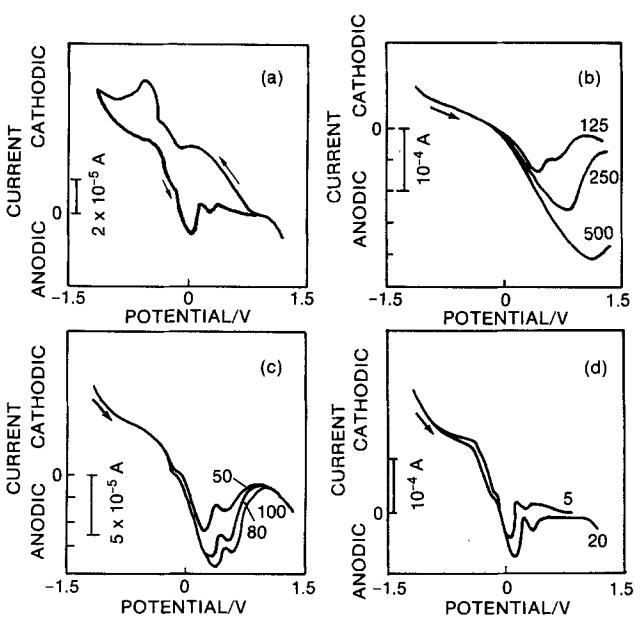

Fig. 9. Effect of ν_{ox} on the shape of oxidative lsv's for $\nu_{red} = 10$ mV s^{-1} and terminated at −1200 mV (*vs.* Ag/AgCl in the same solution). (a) $\nu_{red} = \nu_{ox} = 10$ mV s^{-1}; (b) $\nu_{ox} > 125$ mV s^{-1}; (c) $50 < \nu_{ox} < 100$ mV s^{-1}; (d) $\nu_{ox} < 20$ mV s^{-1}. Electrolyte; 3.0M $AlCl_3$ in $SOCl_2$.

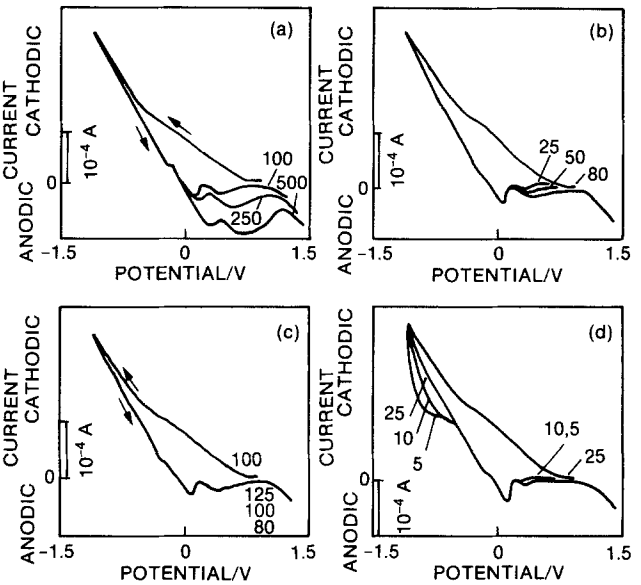

Fig. 10. Effect of ν_{ox} on the shape of oxidative lsv's for $\nu_{red} = 100$ mV s^{-1} and terminated at −1200 mV. Electrolyte, 3.0M $AlCl_3$ in $SOCl_2$.

consistent with fast adsorption of species from the reaction layer.

The common feature of oxidative lsv is the appearance of anodic peak currents. These currents indicate the presence of oxidizable substance(s) in an adsorbed state and, most likely, a reversible character of a charge transfer process, Eq. [V]. Their functional dependence, $j = f(\nu)$, is used in the analysis—a linear relationship is associated with adsorption while the square root dependence usually implies an intervention of a diffusional flux in the overall process. Results summarized in Fig. 11 indicate the dominance of adsorption in a 3.0*M* $AlCl_3$ in $SOCl_2$ electrolyte and the participation of diffusion in a 4.0*M* solution.

Sequence of events, their rates, and the nature of intermediates.—The behavior of the Me/$AlCl_3$-$SOCl_2$ system, subject to cathodic polarization is the result of the participation of, at least, three species, A_2^+, P_1, and P_2. Of these species, the onium ion, A_2^+, is adsorbed rapidly on the

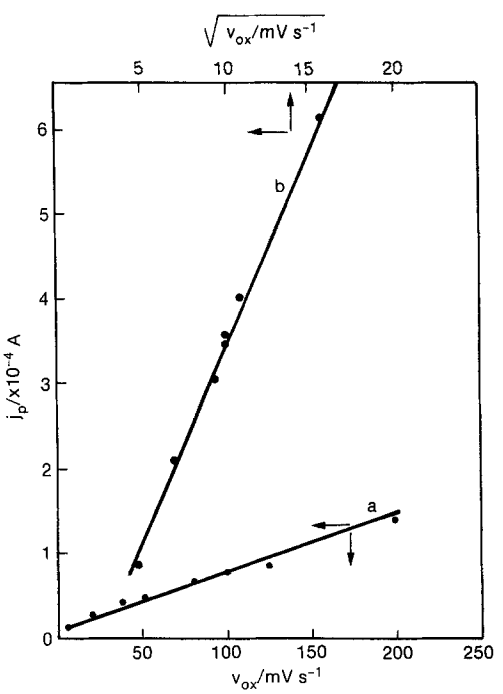

Fig. 11. Plots of anodic peak currents as a function of sweep rate. Curve a, for 3.0M $AlCl_3$ in $SOCl_2$; curve b, for 4.0M $AlCl_3$ in $SOCl_2$.

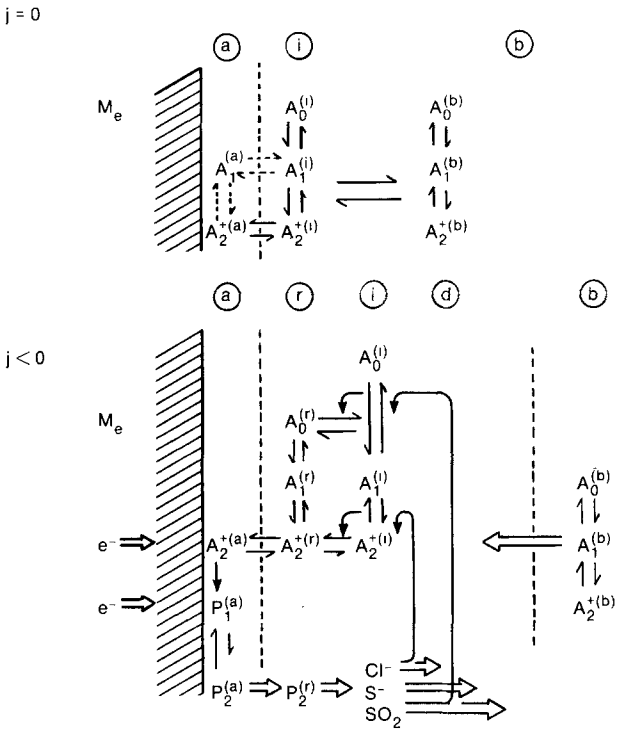

Fig. 12. Summary of participating elementary processes during $SOCl_2$ electroreduction. Superscripts defined in text.

electrode surface, so that its surface concentration is independent of the scan rate. The presence of adsorbed species modifies the *j/V* relationship which, in turn, makes the interpretation of voltammograms more difficult and the identification of participating processes less certain. The separation of anodic peaks at lower scan rates, shown in *e.g.*, Fig. 10b, is indicative of surface coverage by more than a single species (28). The cross over of the reverse scan, *cf.* Fig. 2d and 3b, implies that the standard potential of reaction, Eq. [VI], is more positive than for the first electron transfer, Eq. [V], *i.e.*, $V_2^0 > V_i^0$.

The summary of events associated with the electroreduction of $SOCl_2$ in the $AlCl_3$-$SOCl_2$ system is presented in Fig. 12. Initially, at rest potential, the interphase is equilibrated with the bulk, Eq. [I]-[III], with a significant enrichment of A_1 and A_2^+ in the vicinity of the electrode surface. The interphase consists of adsorption and enrichment layers in contact with the bulk electrolyte.

Upon cathodic polarization, the composition of the interphase includes: $P_1^{(a)}$, $P_1^{(r)}$, $P_2^{(a)}$, $P_2^{(r)}$ with $k_{-2} >> k_2$. The composition of the interphase is now governed by the charge transfer processes. Eq. [V] and [VI], transport from the bulk and desorption from the electrode surface. The enrichment layer, defined in the absence of the charge transfer, becomes the reaction layer, where species P_1 and P_2, stabilized by the adsorption, undergo chemical reaction(s) to yield stable species Cl^-, S, and SO_2. These species interact with the components of the interphase, diffuse to the bulk where they may affect the established equilibria.

Conclusions

1. Because of the reactivity of $SOCl_2$ molecules, study of its electroreduction must consider the nature of the electrolyte.

2. Reduction occurs via the two-electron transfer of which the first is irreversible while the second is quasi-reversible with $k_{-2} >> k_2$ and V_2^0 more positive than V_1^0.

3. Adsorption processes play a key role in the reduction mechanism, giving rise to mild autocatalytic effects. Diffusional processes modify the adsorption characteristics.

4. Chemical reactions, including the formation of stable products occur within the interphase region. Desorption destabilizes intermediate species.

Acknowledgments

This work was supported, in part, by the Office of Naval Research. The authors wish to acknowledge discussions with Dr. R. D. Boss, Naval Ocean Systems, San Diego, California and Dr. J. R. Driscoll, Lockheed—Palo Alto Research Laboratory, Palo Alto, California.

Manuscript submitted Sept. 12, 1988; revised manuscript received Jan. 5, 1989.

The Naval Oceans System Center assisted in meeting the publication costs of this article.

REFERENCES

1. N. Doddapaneni, Abstract 315, p. 505, The Electrochemical Society Extended Abstracts, Vol. 82-2, Detroit, MI, Oct. 17-21, 1982.
2. B. Carter, R. Williams, F. Tsay, A. Rodrigues, and H. Frank, in "Proceedings of 17th IECEC Conference," Vol. 2, Paper Nr N.829110, Los Angeles, CA, 1980.
3. W. A. Bowden and A. N. Dey, *This Journal*, **127,** 1419 (1980).
4. W. K. Istone and R. J. Brodd, *ibid.*, **129,** 1863 (1982).
5. M. J. Madou, J. J. Smith, and S. Szpak, *ibid.*, **134,** 2794 (1987).
6. M. J. Madou and S. Szpak, *ibid.*, **131,** 2471 (1984).
7. R. J. Nowak, D. R. Rolison, J. J. Smith, and S. Szpak, *Electrochim. Acta*, **33,** 1313 (1988).
8. J. J. Smith, S. Pons, J. Li, W. West, and S. Szpak, Paper SW-2 presented at 3rd International Meeting on Li Batteries, Kyoto, Japan, May 1986.
9. P. A. Mosier-Boss, S. Szpak, J. J. Smith, and R. J. Nowak, Abstract 487, p. 695, The Electrochemical Society Extended Abstracts, Vol. 88-1, Atlanta, GA, May 15-20, 1988.
10. S. Szpak and H. V. Venkatasetty, *This Journal*, **131,** 961 (1984).
11. P. A. Mosier-Boss, R. D. Boss, S. Szpak, J. J. Smith, and R. J. Nowak, *J. Chem. Soc., Farad. Trans. 1*, **85,** 11 (1989).
12. P. A. Mosier-Boss, S. Szpak, J. J. Smith and R. J. Nowak, This Journal, **136,** 1282 (1989).
13. J. K. Foley and S. Pons, *Anal. Chem.*, **57,** 945A (1985).
14. C. J. Gabriel, P. A. Mosier-Boss, and S. Szpak, *Spectrochim. Acta*, **43A,** 1293 (1987).
15. B. E. Conway, "Theory and Principles of Electrode Processes," The Ronald Press, New York (1965).
16. I. Lindquist, "Inorganic Adducts of Oxo-Compounds," Academic Press, Inc., New York (1963).
17. W. West, J. J. Smith, and S. Szpak, Paper SW-8 presented at 3rd International Meeting on Li Batteries, Kyoto, Japan, May 1986.
18. P. van Rysselberghe, in "Modern Aspects of Electrochemistry," Vol. 4, J. O'M. Bockris, Editor, Plenum Press, New York (1966).
19. F. A. Cotton and R. Francis, *J. Am. Chem. Soc.*, **82,** 2986 (1960).
20. J. Selbin, W. E. Bull, and L. H. Holmes, *J. Inorg. Nucl. Chem.*, **16,** 219 (1961).
21. J. M. Saveant and E. Vianello, *Electrochim. Acta*, **12,** 629 (1967).
22. C. P. Andrieaux, L. Nadjo, and J. M. Saveant, *J. Electroanal. Chem.*, **26,** 147 (1970).
23. D. F. Milner and M. J. Weaver, *Anal. Chim. Acta*, **198,** 245 (1987).
24. E. Ahlberg and V. D. Parker, *J. Electroanal. Chem.*, **121,** 57 (1981).
25. A. S. Hinman, S. Pons, and J. Cassidy, *Electrochim. Acta*, **30,** 89 (1985); *ibid.*, **30,** 95 (1985).
26. P. van Rysselberghe, "Thermodynamics of Irreversible Processes," Hermann, Paris (1963).
27. S. Srinivasan and E. Gileadi, *Electrochim. Acta*, **11,** 321 (1966).
28. E. Laviron, *J. Electroanal. Chem.*, **52,** 355 (1974).